Figure S1

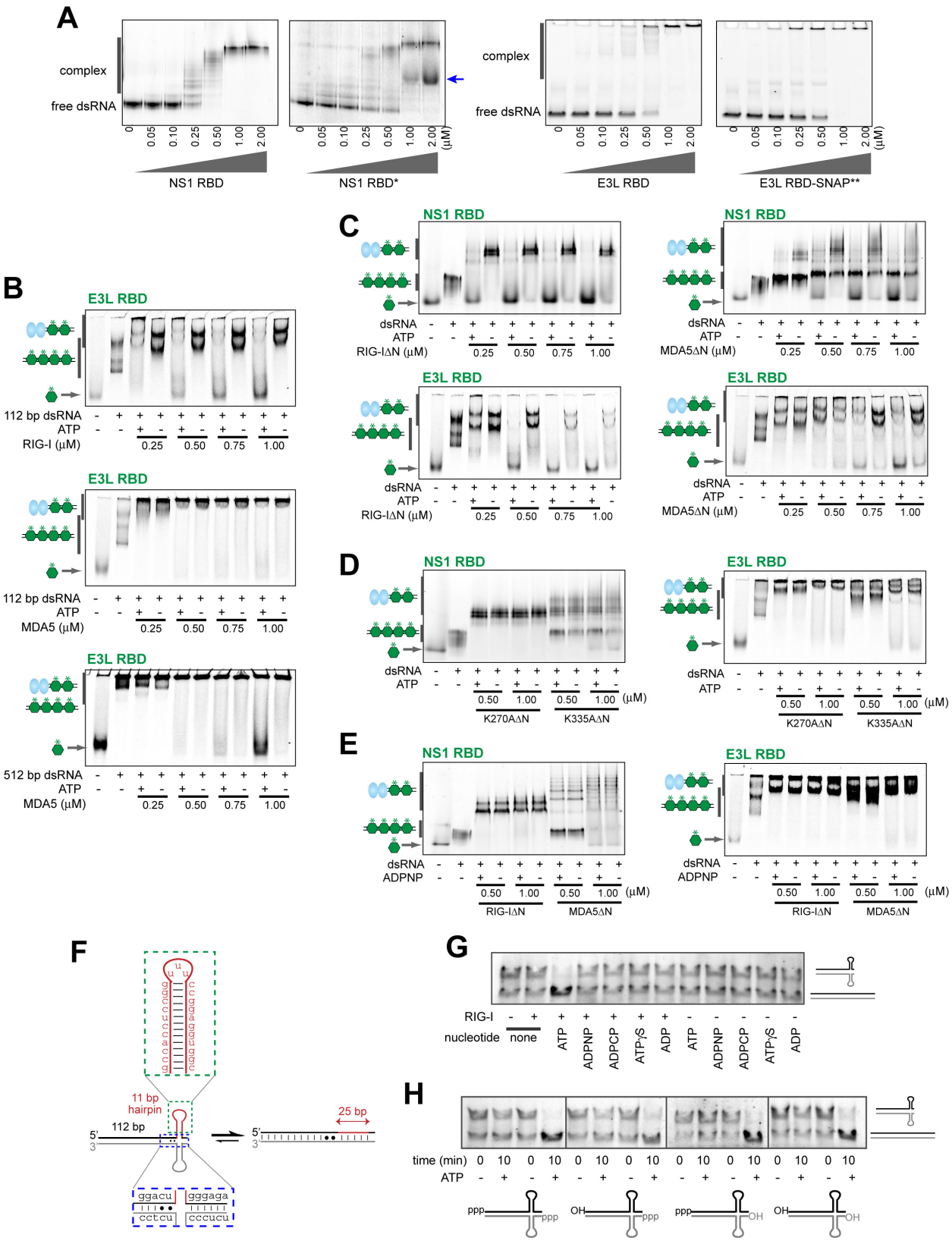
A
complex
free dsRNA
0 0.05 0.10 0.25 0.50 1.00 2.00 (μM)
NS1 RBD
NS1 RBD*
E3L RBD
E3L RBD-SNAP**
B
E3L RBD
112 bp dsRNA
ATP
RIG-I (μM)
0.25 0.50 0.75 1.00
MDA5 (μM)
512 bp dsRNA
C
NS1 RBD
dsRNA
RIG-IΔN (μM)
MDA5ΔN (μM)
D
K270AΔN
K335AΔN
E
ADPNP
RIG-IΔN
MDA5ΔN
F
11 bp hairpin
112 bp
25 bp
5'
3'
ggacu
gggaga
ccucu
cccucu
G
RIG-I
nucleotide
none
ATP
ADPNP
ADPCP
ATPγS
ADP
H
time (min)
0 10 0 10 0 10 0 10 0 10 0 10 0 10 0 10
ppp
OH

Figure S2

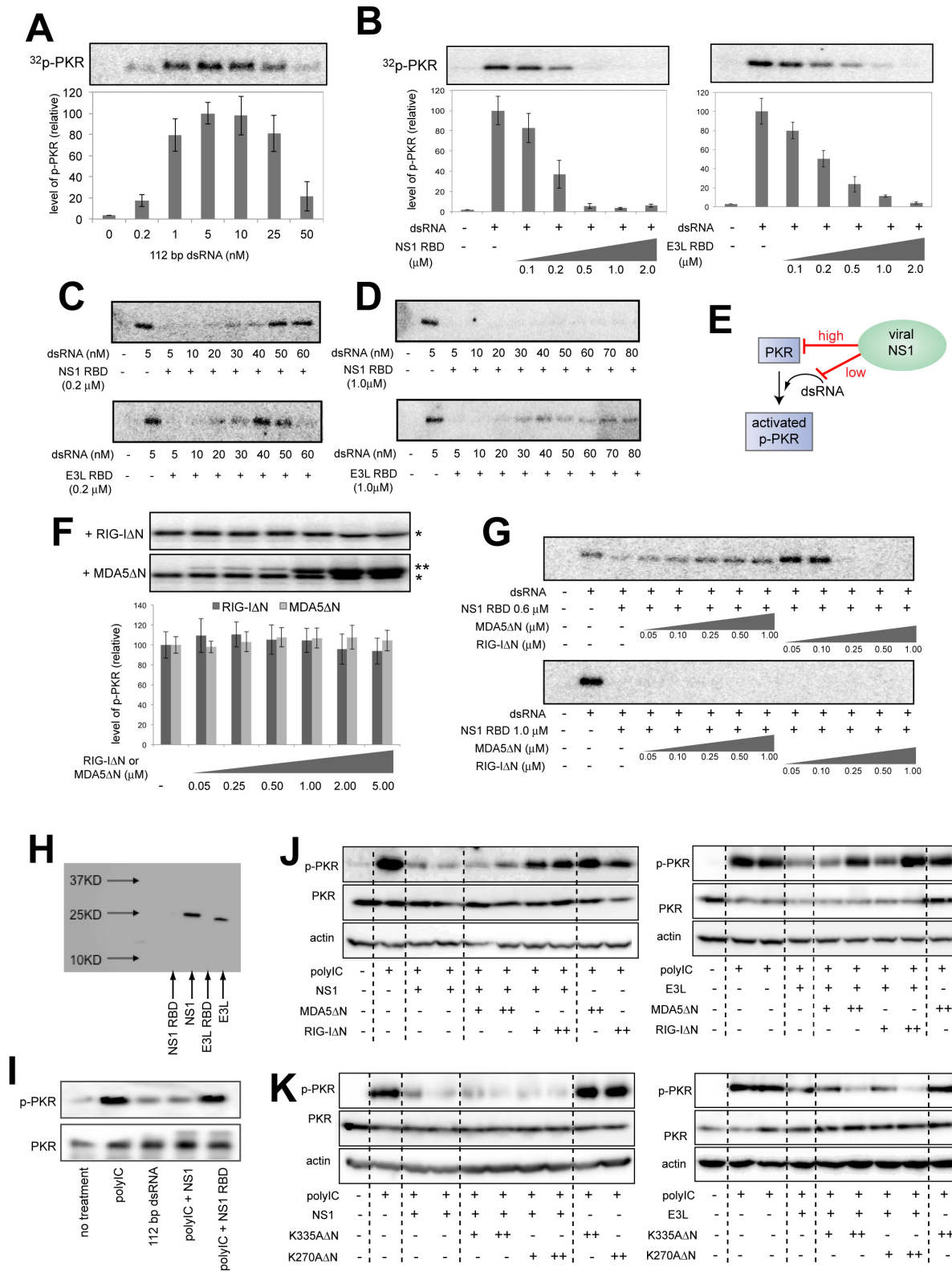
A
32p-PKR
level of p-PKR (relative)
112 bp dsRNA (nM)
B
dsRNA
NS1 RBD (μM)
E3L RBD (μM)
C
dsRNA (nM)
NS1 RBD (0.2 μM)
E3L RBD (0.2 μM)
D
NS1 RBD (1.0μM)
E3L RBD (1.0μM)
E
PKR
high
low
viral NS1
dsRNA
activated p-PKR
F
+ RIG-IΔN
+ MDA5ΔN
RIG-IΔN
MDA5ΔN
RIG-IΔN or MDA5ΔN (μM)
G
NS1 RBD 0.6 μM
NS1 RBD 1.0 μM
MDA5ΔN (μM)
RIG-IΔN (μM)
H
37KD
25KD
10KD
NS1 RBD
NS1
E3L RBD
E3L
I
p-PKR
PKR
no treatment
polyIC
112 bp dsRNA
polyIC + NS1
polyIC + NS1 RBD
J
actin
polyIC
NS1
E3L
MDA5ΔN
RIG-IΔN
K
K335AΔN
K270AΔN

Figure S3

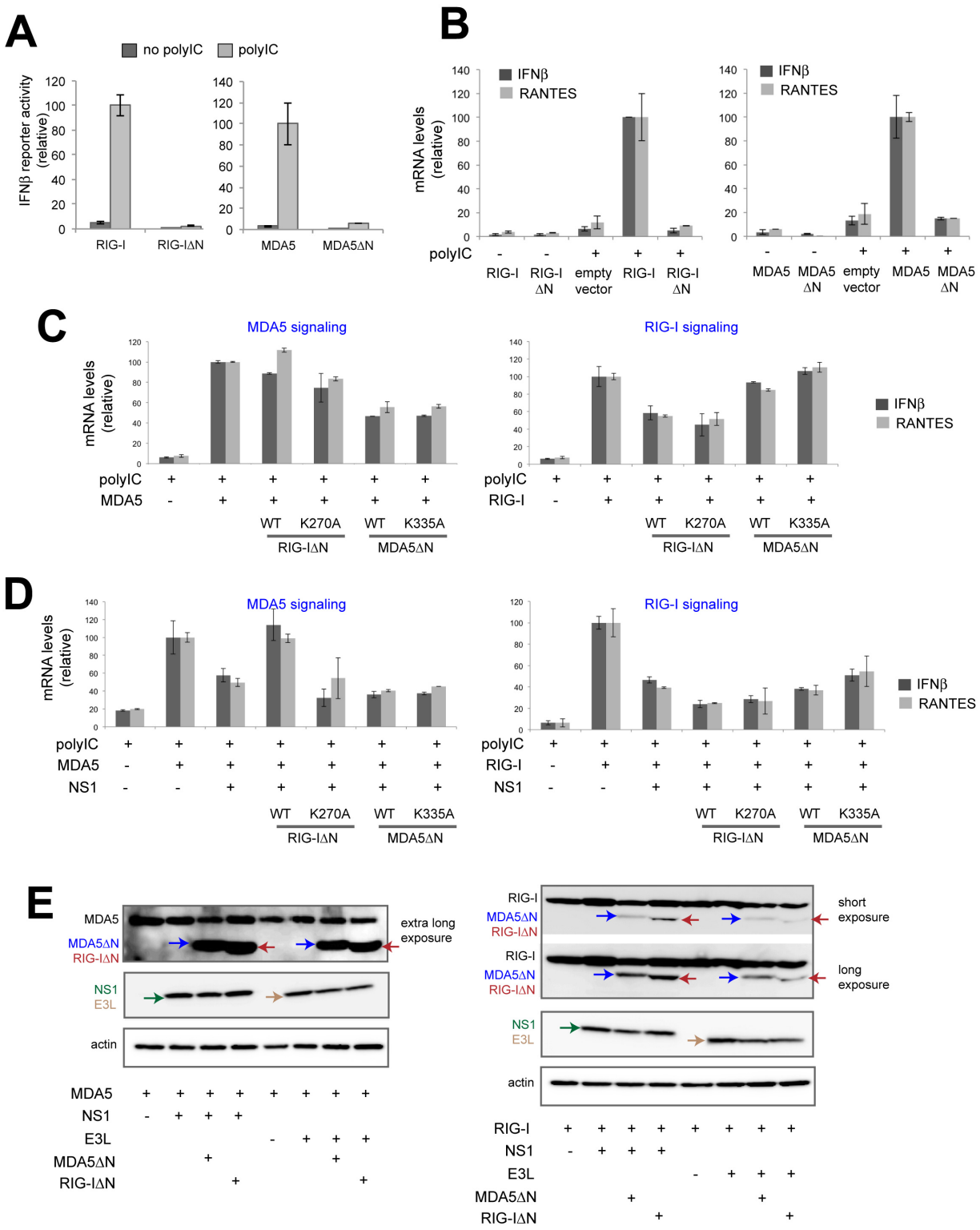
A
no polyIC
polyIC
IFNβ reporter activity (relative)
RIG-I
RIG-IΔN
MDA5
MDA5ΔN
B
IFNβ
RANTES
mRNA levels (relative)
polyIC
RIG-I
RIG-I ΔN
empty vector
MDA5
MDA5 ΔN
C
MDA5 signaling
RIG-I signaling
mRNA levels (relative)
polyIC
MDA5
RIG-I
WT
K270A
K335A
RIG-IΔN
MDA5ΔN
D
MDA5 signaling
RIG-I signaling
mRNA levels (relative)
polyIC
MDA5
RIG-I
NS1
E
MDA5
MDA5ΔN
RIG-IΔN
extra long exposure
NS1
E3L
actin
E3L
short exposure
long exposure

Figure S4

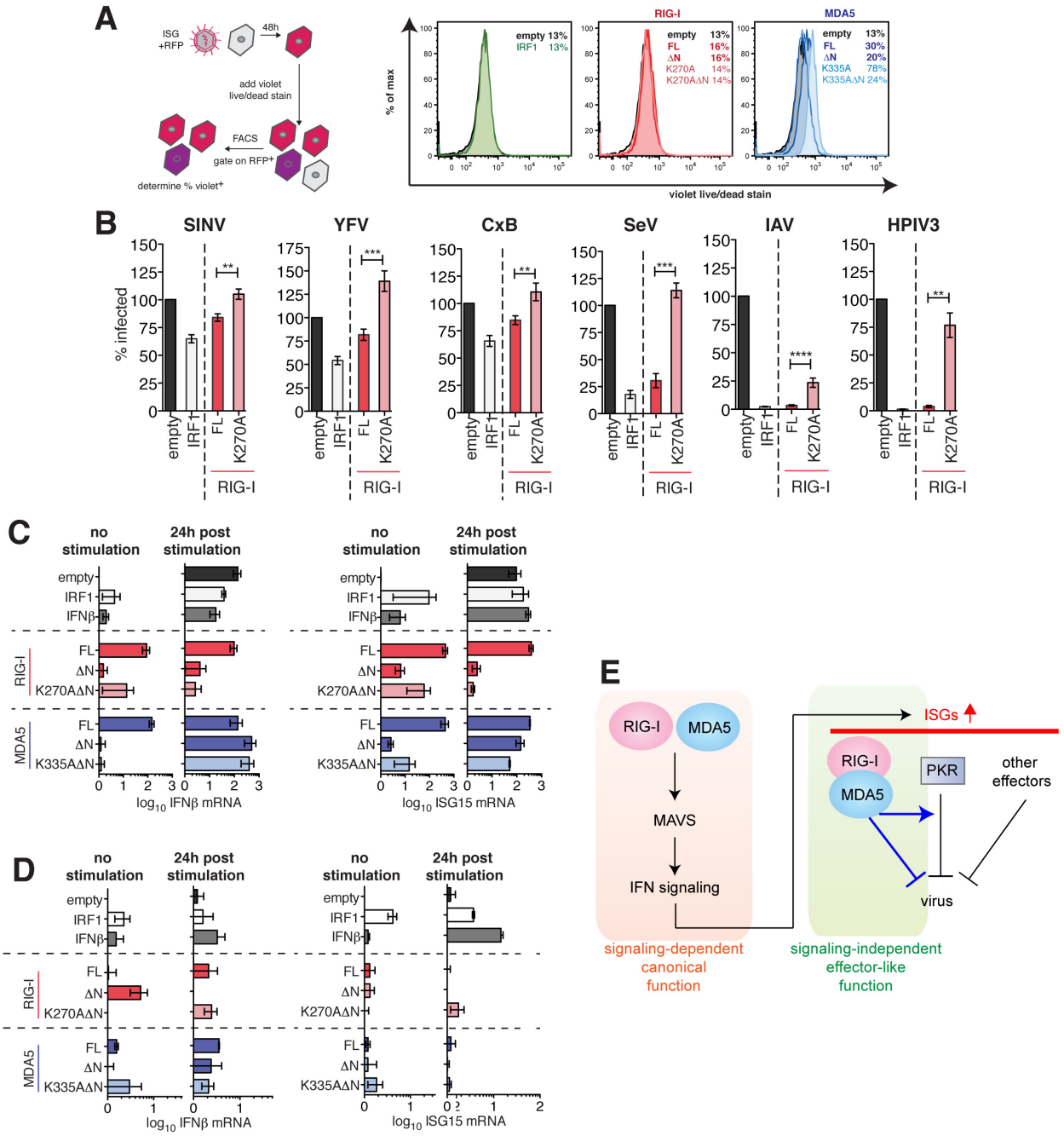
A
ISG +RFP
48h
add violet live/dead stain
FACS
gate on RFP+
determine % violet+
% of max
violet live/dead stain
RIG-I
MDA5
empty 13%
IRF1 13%
FL 16%
ΔN 16%
K270A 14%
K270AΔN 14%
FL 30%
ΔN 20%
K335A 78%
K335AΔN 24%
B
SINV
YFV
CxB
SeV
IAV
HPIV3
% infected
empty
IRF1
FL
K270A
RIG-I
C
no stimulation
24h post stimulation
IFNβ
ΔN
K270AΔN
K335AΔN
MDA5
log10 IFNβ mRNA
log10 ISG15 mRNA
D
E
MAVS
IFN signaling
ISGs
PKR
other effectors
virus
signaling-dependent canonical function
signaling-independent effector-like function

Supplementary Figure Legends

Figure S1 RIG-I and MDA5 can displace viral proteins bound to dsRNA in an ATP hydrolysis-dependent manner. Related to Figure 1.

A. dsRNA binding activities of recombinant NS1 and E3L RNA binding domains (RBDs) as measured by electrophoretic mobility shift assays (EMSA). NS1 RBD was labeled with fluorescein (*) using a protein ligase, sortase (see Method). E3L RBD was labeled with Alexa647 (**) using a fusion tag, SNAP (NEB). The 112 bp dsRNA was incubated with an increasing amount of RBDs and their complex formation was analyzed by 4-12% Bis-Tris native PAGE (Life) for NS1 and 4-20% TBE gel (Life) for E3L. Similar RNA binding activities were observed between unlabeled and fluorescently labeled proteins. The gel images were obtained by SybrGold stain (Life) of dsRNA. The arrow indicates fluorescein-labeled free NS1 RBD, which was also visible due to the spectral overlap between SybrGold and fluorescein.

B. Gel analysis showing the displacement of E3L RBD from 112 bp or 512 bp dsRNA by RIG-I/MDA5. The experiments were performed as described in Figures 1A-B. Gel images were obtained using the Alexa 647 labeled E3L RBD-SNAP fusion protein. For results with NS1 RBD, see Figure 1B.

C. Viral protein displacement assay using RIG-IΔN/MDA5ΔN and 112 bp dsRNA. The experiments were performed as in Figures 1A-B.

D. Viral protein displacement assay using the catalytic mutants of RIG-IΔN (K270A) and MDA5ΔN (K335A) in the presence and absence of ATP.

E. Viral protein displacement assay using RIG-IΔN and MDA5ΔN in the presence and absence of ADPNP.

F. Details of the dsRNA with complementary hairpins (used in Figure 1I). To suppress spontaneous relaxation of the hairpins, two mismatches (•) were introduced just upstream of the hairpin. The sequence of the 112 bp region was derived from the first 112 bp of the MDA5 gene.

G. The hairpin relaxation assay in the presence or absence of ATP or non-hydrolyzable ATP analogs. The assay was performed as in Figure 1I.

H. The hairpin relaxation assay using dsRNA formed by a combination of CIP-treated and untreated strands.

Figure S2 RIG-IΔN and MDA5ΔN relieve the viral suppression of PKR. Related to Figure 2.

A. PKR autophosphorylation activity assay using [γ-^{32}P]-ATP. PKR (0.2 μM) was stimulated with indicated amount of 112 bp dsRNA and its autophosphorylation was detected by SDS-PAGE. The bell-shaped dependence on dsRNA concentration is consistent with previous reports (Lemaire et al., 2005). Data are shown in mean ± SD (n=3).

B. PKR inhibition by NS1 RBD and E3L RBD. PKR (0.2 μM) was stimulated with 112 bp dsRNA (5 nM) in the presence of increasing concentrations of NS1 RBD or E3L RBD. Data are shown in mean ± SD (n=3).

C. PKR inhibition by NS1 and E3L RBDs (0.2 μM) and its relief by an excess amount of 112 bp dsRNA. This result suggests that NS1 and E3L RBDs suppress PKR primarily through sequestering dsRNA under these conditions.

D. Same as (C) but with NS1 and E3L RBDs (1.0 μM). PKR inhibition by NS1 RBD (1.0 μM) could not be relieved with an excess amount of dsRNA, suggesting that NS1 RBD at this concentration suppresses PKR through both dsRNA-dependent and -independent mechanisms (Li et al., 2006).

E. Schematic summarizing the result from (C-D). “high” and “low” indicate high (1.0 μM) and low (0.2 μM) concentrations of NS1.

F. The effect of RIG-IΔN and MDA5ΔN on the autophosphorylation activity of PKR. PKR (0.2 μM) was stimulated with 112 bp dsRNA (5 nM) in the presence of increasing concentrations of RIG-IΔN or MDA5ΔN. The result shows that RIG-IΔN and MDA5ΔN have little inhibitory effect on PKR, which may reflect either that RIG-IΔN and MDA5ΔN do not displace PKR or that RIG-IΔN and MDA5ΔN displace PKR, but transient exposure to dsRNA is sufficient for

activation of PKR. * and ** indicate phosphorylated PKR and MDA5ΔN, respectively. Data are shown in mean ± SD (n=3).

G. Impact of RIG-IΔN and MDA5ΔN on the suppression of PKR by NS1 RBD. Experiments were performed as in Figure 2A, but with higher concentrations of NS1 RBD (top: 0.6 μM and bottom: 1 μM, as opposed to 0.2 μM in Figure 2A). The result shows that while RIG-IΔN and MDA5ΔN can relieve the suppression of PKR by NS1 RBD at 0.2 or 0.6 μM, where NS1 RBD inhibits PKR primarily by dsRNA sequestration, they cannot relieve the suppression at 1 μM where the dsRNA-independent mechanism becomes dominant. Note that the inhibition of PKR by 0.6 μM of NS1 RBD was relieved by RIG-I at concentration below, but not above, 0.25 μM. This suggests that at higher concentrations of RIG-I (≥0.25 μM), the positive effect of RIG-I on PKR through displacement of NS1 is compensated by its negative effect (possibly through competition for dsRNA or displacement of PKR). This is unlike the situation without NS1 RBD (Figure S2F) or with 0.1 μM of NS1 RBD (Figure 2A), where RIG-I exerts little inhibitory effect on PKR over a wide range of concentration. Together, these results suggest more complex picture of the interplays among PKR, RIG-I and NS1.

H. Western blot analysis of expression of FLAG-tagged NS1 (26 kDa), E3L (22 kDa) and their RBDs (~10 kDa).

I. Stimulation of PKR autophosphorylation in 293T cells by polyIC or *in vitro* transcribed 112 bp dsRNA in the presence or absence of full-length NS1 or NS1 RBD. Due to limited stimulation of PKR by 112 bp dsRNA, we used polyIC in cellular analysis.

J. Impact of RIG-IΔN and MDA5ΔN on the PKR autophosphorylation activity in cells. 293T cells were stimulated with polyIC in the presence or absence of ectopically expressed full-length NS1/E3L, and the effect of RIG-IΔN or MDA5ΔN were examined. The level of endogenous p-PKR was measured by anti-phospho PKR western blot.

K. Same as (J) using the catalytic mutants of RIG-IΔN and MDA5ΔN (K270AΔN and K335AΔN, respectively).

Figure S3 RIG-IΔN relieves the viral suppression of the MDA5 signaling activity. Related to Figure 3.

A. IFNβ reporter activities of RIG-I, MDA5 and their 2CARD deletion mutants (ΔNs) with or without polyIC stimulation in 293T cells. Data are shown in mean ± SD (n=3).

B. qRT-PCR analysis of the levels of IFNβ and RANTES mRNAs induced by RIG-I, MDA5 and their ΔN truncation mutants in the presence or absence of polyIC in 293T cells. Data are shown in mean ± SD (n=3).

C. qRT-PCR analysis of the levels of IFNβ and RANTES mRNAs induced by full-length MDA5/RIG-I in the presence or absence of wild-type or catalytic mutants of RIG-IΔN and MDA5ΔN. Data are shown in mean ± SD (n=3).

D. Same as (C) except in the presence of NS1. Data are shown in mean ± SD (n=3).

E. Western blot analysis of FLAG-tagged RIG-I, MDA5, RIG-IΔN, MDA5ΔN, NS1 and E3L when expressed as in Figure S3D. Due to different expression levels, different exposure times were used. The result confirms that the levels of full-length RIG-I and MDA5 were largely unaffected by co-expression of NS1/E3L and RIG-IΔN/MDA5ΔN.

Figure S4 Gene induction and cytotoxicity profiles. Related to Figure 4.

A. Cytotoxicity profiles of A549 cells transduced to express full-length (FL) wild-type RIG-I, MDA5 or their 2CARD truncation (ΔN) variants. 48h post transduction, cells were treated with violet live/dead stain and the number of dead (violet) cells in the RFP^+ population was analyzed by flow cytometry. The toxic effect of K335A has prevented analysis of its antiviral potency using viral spread assay.

B. Image-based viral spread assay on A549 cells, comparing the antiviral potency of RIG-I and K270A. Experiments were performed as in Figure 4A. While the data show the importance of ATP-hydrolysis in antiviral potency of RIG-I, this cannot be solely attributed to the protein-

displacement activity of RIG-I, as ATP hydrolysis is also important for oligomerization of 2CARD (Jiang et al., 2012; Peisley et al., 2013), which is a pre-requisite for MAVS activation. Thus, to evaluate the importance of the signaling-independent protein-displacement activity, we compared RIG-IΔN and K270AΔN instead (in Figure 4A).

C. ISG induction profiles in A549 cells. Cells were transduced to express RIG-I, MDA5 or their ΔN variants and stimulated with IFNβ or infected with HPIV3 at MOI=1 for 24h. The levels of mRNAs for IFNβ and ISG15 were determined by qRT-PCR. Values were normalized to housekeeping gene RPS11 and to unstimulated empty control. Indicated pairs were analyzed by Mann Whitney test. ns = not significant. ****p<0.0001, ***p<0.001, **p<0.01, *p<0.1. Note that expression of RIG-IΔN ad K270AΔN decreased ISG induction 24 hr post stimulation (as compared to the empty control), possibly reflecting the abilities of ΔNs to sequester viral dsRNAs from endogenous RIG-I/MDA5. This dominant negative effect of RIG-IΔN further adds the significance of the observed antiviral activity of RIG-I ΔN against HPIV3 (Figure 4A). This suppressive effect of ΔNs on IFN signaling could also explain the apparent proviral effect of K270AΔN on YFV and SeV (Figure 4A).

D. ISG induction profiles in 293T $MAVS^{-/-}$ cells. Experiments were performed as in (C).

E. Model for the dual functions of RIG-I/MDA5 as canonical pattern recognition receptors and effector molecules. We propose that the canonical receptor function in viral RNA recognition and IFN signaling dominates at baseline, whereas the effector-like function emerges when RIG-I and MDA5, along with other effector molecules, are induced by IFN. The ability of RIG-I and MDA5 to remodel ribonucleoprotein complexes may assist functions of other ISGs, such as PKR (by exposing viral dsRNA), or may directly interfere with core viral life cycle steps.

Extended Experimental Procedures

Material preparation

Plasmids Plasmids for human RIG-I, MDA5 and their variants were described previously (Peisley et al., 2011; Wu et al., 2014). Briefly, pET50 was used for recombinant protein expression (Peisley et al., 2012; Peisley et al., 2011), and pFLAG-CMV4 was used for expression in mammalian cells (Wu et al., 2013; Wu et al., 2014). Full-length NS1 of influenza A virus (PR8) and full-length E3L of vaccinia virus (Western Reserve) were subcloned between the EcoRI and KpnI restriction sites in pFLAG-CMV4. The RBDs for Influenza A NS1 (residue 1-83), vaccinia E3L (96-191) and their variants were subcloned between KpnI and EcoRI in pET47b. Human PKR was subcloned between KpnI and HindIII in pET47b and λ protein phosphatase (λPPase) was expressed from pET11b (a gift from Dr. James Cole, University of Connecticut).

Proteins Human RIG-I, MDA5 and their variants were purified as previously reported (Peisley et al., 2011). Briefly, proteins were expressed in BL21(DE3) at 20˚C for 16-20 hr following induction with 0.5 mM IPTG. Cells were lysed by high pressure homogenization using an Emulsiflex C3 (Avestin), and proteins were purified by a combination of Ni-NTA and heparin affinity chromatography and size exclusion chromatography (SEC) in 20 mM Hepes, pH 7.5, 150 mM NaCl and 2 mM DTT. PKR was co-expressed with λPPase in BL21(DE3) supplemented with the Rosetta2 plasmid (Novagen), and purified using the published protocol (McKenna et al., 2007), with an exception of using a high salt concentration (1 M NaCl) after lysis and during the entire purification procedure with the final SEC in 50 mM Tris, pH 8.0, 0.3 M NaCl, 0.5 mM EDTA. NS1 RBD, E3L RBD and their SNAP-fusion proteins were expressed in BL21(DE3) at 20˚C for 16-20 hr following induction with 0.5 mM IPTG. Cells were lysed in 50 mM sodium phosphate, pH 8.0, 0.5M NaCl, 10% glycerol, 20mM imidazole, 5mM BME, 0.5 mM PMSF by Emulsiflex, and proteins were purified by Ni-NTA affinity purification and SEC in 50mM Tris pH 7.5, 1M NaCl, 0.5 mM EDTA. While E3L RBD fused to a SNAP-tag showed comparable dsRNA affinity as with E3L RBD, NS1 RBD-SNAP did not bind dsRNA. Thus, NS1 RBD was fluorescently labeled at the

N-terminus using a protein ligase, sortase (Antos et al., 2009). Purified protein (~5 mg/ml) was incubated with 0.5 mM peptide (LPETGG) conjugated with fluorescein (Anaspec) and 0.3 mM *S. aureus* sortase A (the expression plasmid was obtained from the Hidde Ploegh lab, MIT) (Antos et al., 2009) at room temperature (RT) for 4-6 hr, followed by Ni-NTA affinity purification and SEC to remove sortase and unlabeled dye, respectively. The labeled protein was functional as measured by the dsRNA binding EMSA (Figure S1A).

RNAs The sequence of 112 bp and 512 bp dsRNA were derived from the first 100 bp and 500 bp of the MDA5 gene, respectively, flanked by 5'gggaga and tctccc3'. The sequence of the hairpin RNA was shown in Figure S1F. All RNAs were prepared by T7 in vitro transcription and PAGE purification as previously described (Peisley et al., 2011). The 112 bp dsRNA used for the streptavidin displacement assay was prepared by annealing two RNA strands, where one strand was labeled with 3'-biotin and the other with 3'-fluorescein. For 3' labeling, RNA was oxidized with 0.1 M sodium meta-periodate (Pierce) overnight in 0.1 M NaOAc pH 5.4. The reaction was quenched with 250 mM KCl, buffer exchanged using desalting columns into 0.1 M NaOAc pH 5.4 and further incubated with 0.1 M fluorescein-5-thiosemicarbazide (Life), Cy3-hydrazide (GE) or Biotin-hydrazide (Pierce) for ~4-6 hr at RT. For hairpin containing dsRNA, two strands of hairpin containing dsRNA were separately prepared, annealed at RT for 5 min, and immediately used for the assay. One of the two RNA strands was labeled with 3'-fluorescein prior to annealing. For dephosphorylation of 5'ppp, 2 μg of RNAs were treated 5 unit of CIP (NEB) for 10 min at 37˚C and re-purified using QIAquick Nucleotide removal kit.

Cells The MAVS$^{-/-}$ and STAT1$^{-/-}$ 293T cells were generated using the TALEN technology. We utilized the target site 5'-TTGCTGAAGACAAGACCTAT / AAGTATATCTGCCGC / AATTTCAGCAATTTTTGCAA-3' for MAVS and 5'-TTCTAACCACTGTGCCAGGT / ACTGTCTGATTTCC / ATGGGAAAACTGTCATCATA-3' for STAT1 (Schmid-Burgk et al., 2013). Each pair of TALEN plasmids were transfected into 293T cells at a ratio of 1:1 using GeneJuice (Merk Millipore). Two days after transfection cells were diluted to 10 cells/ml and plated in 96 well plates (100μl per well) to obtain single cell clones. After two weeks of growth, single cell clones were picked

and expanded in two independent culture vessels. One vessel was lysed and genotyped as previously described (Schmid-Burgk et al., 2014). Knockout clones were identified by the presence of all-allelic frame shift indels, and confirmed by western blots using anti-STAT1 (Cell Signaling) or anti-MAVS (Bethyl labs) antibodies.

Viruses To generate lentiviruses, RIG-I, MDA5 and their variants were first subcloned into pCR®8/GW/TOPO® TA (Life Technologies), and then subcloned into pSCRPSY lentiviral vector co-expressing RFP and a puromycin resistance gene. Lentivirus particles were generated with standard protocols on 293T cells. Human parainfluenza virus 3 – EGFP was a gift from Peter Collins, NIAID, NIH, and amplified in Vero cells under serum-free conditions (OptiPro media). Sendai virus expressing EGFP was obtained from Dr. Dominique Garcin (University of Geneva) and amplified in 10d embryonated hen eggs. Yellow fever YF17D(5'C25Venus2AUbi) reporter virus (Jones et al., 2010) was grown on BHK-J cells. Coxsackievirus B reporter virus CVB3-EGFP (Feuer et al., 2002) was obtained from Dr. Lindsay Whitton (The Scripps Research Institute), and amplified on Vero cells. Toto1101-strain-based Sindbis reporter virus (TE/5'2J/GFP) (Law et al., 2010) was grown on BHK-J cells. Non-reporter influenza virus A/WSN/33(H1N1) was grown on MDCK cells. The non-reporter IAV was chosen over the reporter strains (such as A/PuertoRico/8/1934-NS1-GFP) because these reporter viruses eliminated the fluorescent protein from two rounds of infection (data not shown), which prevented viral spread assays.

Antibodies Following antibodies were used to confirm the expression of FLAG-tagged proteins: anti-FLAG M2-HRP (A8592, Sigma), anti-beta-actin (8457S, Cell Signaling), anti-rabbit IgG, HRP-conjugated (7074P2, Cell Signaling). For confirmation of MAVS and STAT1 knockout, we used anti-MAVS (A300-782A, Bethyl Laboratories Inc.) and anti-STAT1 (#9172, Cell Signaling Technology).

Protein displacement, streptavidin displacement and hairpin removal assays

For protein displacement assay, dsRNA (45 nM) was pre-incubated with fluorescently labeled viral RBDs (1 μM, fluorescein-labeled NS1 RBD and Alexa 647 labeled E3L RBD-SNAP) in 20 mM Hepes,

pH 7.5, 100 mM NaCl, 1.5 mM MgCl2 and 2 mM DTT at 37˚C for 5 min. The RBD:dsRNA complex was further incubated with an indicated amount of RIG-I/MDA5 with or without 2 mM ATP or ADPNP) at 37˚C for 5 min. The reaction was quenched with 10 mM EDTA on ice and was immediately analyzed by 4-12 % Bis-Tris native PAGE (Life). The choice of SNAP-fusion for E3L was to help migration of E3L RBD into the native gel. Fluorescent gel images were recorded using an FLA9000 scanner (GE).

For streptavidin displacement, 3'-biotin, 3'-fluorescein labeled dsRNA (10 nM) was incubated with 1 μM streptavidin at RT for 5 min and subsequently with 300 nM RIG-I or MDA5 in 20 mM Hepes, pH 7.5, 150 mM NaCl, 1.5 mM $MgCl_2$ and 2 mM DTT. The reaction was initiated by the addition of 2 mM ATP and 10 μM free biotin at 37˚C. Free biotin serves as a streptavidin trap to prevent re-binding of displaced streptavidin to biotinylated dsRNA. Aliquots were withdrawn at indicated time points, quenched with 10 mM EDTA on ice, mixed with 2x loading buffer (20 mM HEPES, pH 7.5, 0.6 M NaCl, 0.6% SDS, 1 mg/ml heparin, 0.08% Bromophenol Blue and 20% sucrose), and immediately analyzed on 6% native TBE gels. Note that 0.6% SDS was used to remove RIG-I/MDA5 from dsRNA without disrupting the streptavidin:biotin interaction (Morris and Raney, 1999).

For hairpin removal assay, the hairpin-containing dsRNA was incubated with 300 nM RIG-I/MDA5 with and without ATP at 37˚C for indicated time period, quenched with the same 2x loading buffer as above and immediately analyzed on 6% native TBE gels. The loading buffer induces dissociation of RIG-I and MDA5 from dsRNA without affecting the hairpin stability.

PKR activity assay

Unless mentioned otherwise, 112 bp dsRNA (5 nM) was pre-incubated with unlabeled NS1 RBD (0.2 μM) and E3L RBD (1 μM) in 20 mM Hepes, pH 7.5, 100 mM NaCl, 1.5 mM $MgCl_2$ and 2 mM DTT at 37˚C for 5 min, and was additionally incubated with a mixture of PKR (200 nM), ATP (5 mM, containing ~12.5 μCi/ml [γ-^{32}P]-ATP) and RIG-IΔN or MDA5ΔN (indicated concentrations) at 37˚C for 15 min. The

reaction was quenched with 10 mM EDTA, and analyzed by 10% SDS-PAGE and phosphor imaging using a phosphor storage screen (GE) and FLA9000 scanner (GE).

For cellular assay, 293T cells were transfected with pFLAG-CMV4 plasmids encoding RIG-IΔN or MDA5ΔN (wt or catalytic mutants, indiated amount) and full-length NS1 or E3L (2 μg/ml) using lipofectamine2000 (Life) in 12 well plate at 95% confluence. 24 hr post-transfection, cells were stimulated with high molecular weight polyIC (Invivogen) (1 μg/ml). Cells were harvested 6 hr post-stimulation and lysed in RIPA buffer containing protease inhibitor cocktail (Sigma) and phosphatase inhibitor (1 mM Na_3VO_4 and 10 mM NaF). Activity of endogenous PKR was measured by western blot using PKR Phospho (pT446) antibody (Abcam). Western blots using PKR antibody (Abcam) and actin antibodies (Sigma) were used as internal controls.

IFN-β promoter reporter assay

293T cells were maintained in 48-well plates in Dulbecco's modified Eagle medium (Cellgro) supplemented with 10% heat-inactivated fetal calf serum and 1% penicillin/streptomycin. At ~95% confluence, cells were transfected with pFLAG-CMV4 plasmids encoding NS1 or E3L (2 μg) by using lipofectamine2000 (Life) according to the manufacturer's protocol. Empty vector was used to maintain the total amount of DNA and lipofectamine constant. The medium was changed 6-8 hr after the first transfection and additionally transfected with full-length RIG-I or MDA5 (5 ng), RIG-IΔN or MDA5ΔN (wild-type or catalytic mutants, 5 to 20 ng), IFNβ- promoter driven firefly luciferase reporter plasmid (100 ng), a constitutively expressed Renilla luciferase reporter plasmid (pRL-CMV, 10 ng) and high molecular weight polyIC (0.2 μg, Invivogen). Cells were lysed ~20 hr post-stimulation and IFN-promoter activity was measured using the Dual Luciferase Reporter assay (Promega) and a Synergy2 plate reader (BioTek). Firefly luciferase activity was normalized against Renilla luciferase activity.

qRT-PCR

293T cells were prepared as in the IFN-β promoter reporter assay. Total RNAs were extracted using TRIzol® reagent (Invitrogen) and cDNA was synthesized using High Capacity cDNA reverse transcription kit (Applied Biosystems) according to the manufacture's instruction. Real-time PCR was performed using a SYBR Green Master Mix (Applied Biosystems), the StepOne™ Real-Time PCR Systems (Applied Biosystems) and the following primers: IFNB1 forward 5'-CTTTCGAAGCCTTTGCTCTG-3' and reverse 5'-CAGGAGAGCAATTTGGAGGA-3'; RANTES forward 5'-TACACCAGTGGCAAGTGCTC-3' and reverse 5'-TGTACTCCCGAACCCATTTC-3'; beta-Actin forward 5'-GCACAGAGCCTCGCCTT-3'
and reverse 5'-GTTGTCGACGACGAGCG-3'. The results were normalized against the beta-Actin mRNA level.

Image-based virus spread assays

A549 cells or 293T-based knock-out cell lines were prepared in 96-well format, transduced with lentiviral stocks for 2 days to similar transduction efficiencies, and challenged with different viruses at 100 PFU/well (MOI 0.01). For SeV- and IAV-infections, 1μg/ml TPCK-trypsin was added to the media to enable multicycle replication. Cells were fixed after multiple rounds of replication, until about 10-20% of cells were infected in the empty control. Because of differences in replication time, the endpoint differed for different viruses: CxB at 24hpi; SINV, SeV, IAV, HPIV3 at 48hpi; YFV at 72hpi. Cells were fixed with 8% PFA, permeabilized with TritonX-100 (0.1% in PBS), and stained with DAPI (for all viruses) and IAV NP (Millipore)(for IAV). Fish gelatin (0.2% in PBS) was used as blocking reagent. Four images were taken per well using the ImageXPressMICRO System (Molecular Devices), and analyzed for total (DAPI), transduced (RFP) and infected cells (GFP, Venus, or Alexa488) with MetaXPress software V5.1.0.46.

ISG induction assays

To determine mRNA expression levels, we transduced A549 cells or MAVS$^{-/-}$ or STAT1$^{-/-}$ 293T cells with lentiviral stocks in duplicate for 2d to achieve similar transduction efficiencies. One replicate was then either infected with HPIV3 at MOI=1, or treated with IFN-β (Abcam) at 1pmol/ml. Total RNA was extracted using RNeasy mini kit (Qiagen), and the level of indicated mRNA was measured by qRT-PCR (SuperScript III First Strand Synthesis System, Life Technologies) and SYBR green assay (Roche) as described previously (Marukian et al., 2011), and normalized against the housekeeping gene RPS-11.

Cytotoxicity assays

To determine cytotoxic effect of the expression constructs, we transduced A549 cells for 2 days to yield similar transduction efficiencies. Cells were washed with PBS, and further incubated with violet live/dead stain (Invitrogen) in dark for 30 min at RT. Cells were then washed with PBS, harvested using Accumax cell detachment solution and fixed with 3% PFA in PBS. The percentage of violet-positive cells within the RFP-positive (transduced) population was determined by flow cytometry.

References

Antos, J.M., Chew, G.-L., Guimaraes, C.P., Yoder, N.C., Grotenbreg, G.M., Popp, M.W.-L., and Ploegh, H.L. (2009). Site-specific N- and C-terminal labeling of a single polypeptide using sortase of different specificity. J. Am. Chem. Soc. *131*, 10800-10801.

Feuer, R., Mena, I., Pagarigan, R., Slifka, M.K., and Whitton, J.L. (2002). Cell cycle status affects coxsackievirus replication, persistence, and reactivation in vitro. J. Virol. *76*, 4430-4440.

Jiang, X., Kinch, L.N., Brautigam, C.A., Chen, X., Du, F., Grishin, N.V., and Chen, Z.J. (2012). Ubiquitin-Induced Oligomerization of the RNA Sensors RIG-I and MDA5 Activates Antiviral Innate Immune Response. Immunity *36*, 959-973.

Jones, C.T., Catanese, M.T., Law, L.M., Khetani, S.R., Syder, A.J., Ploss, A., Oh, T.S., Schoggins, J.W., MacDonald, M.R., Bhatia, S.N.*, et al.* (2010). Real-time imaging of hepatitis C virus infection using a fluorescent cell-based reporter system. Nat Biotech *28*, 167-171.

Law, L.M., Albin, O.R., Carroll, J.W., Jones, C.T., Rice, C.M., and MacDonald, M.R. (2010). Identification of a dominant negative inhibitor of human zinc finger antiviral protein reveals a functional endogenous pool and critical homotypic interactions. J. Virol. *84*, 4504-4512.

Lemaire, P.A., Lary, J., and Cole, J.L. (2005). Mechanism of PKR Activation: Dimerization and Kinase Activation in the Absence of Double-stranded RNA. J. Mol. Biol. *345*, 81-90.

Li, S., Min, J.-Y., Krug, R.M., and Sen, G.C. (2006). Binding of the influenza A virus NS1 protein to PKR mediates the inhibition of its activation by either PACT or double-stranded RNA. Virology *349*, 13-21.

Marukian, S., Andrus, L., Sheahan, T.P., Jones, C.T., Charles, E.D., Ploss, A., Rice, C.M., and Dustin, L.B. (2011). Hepatitis C virus induces interferon-λ and interferon-stimulated genes in primary liver cultures. Hepatology *54*, 1913-1923.

McKenna, S.A., Lindhout, D.A., Shimoike, T., and Puglisi, J.D. (2007). Biophysical and Biochemical Investigations of dsRNA-Activated Kinase PKR. Methods in Enz *430*, 373-396.

Morris, P.D., and Raney, K.D. (1999). DNA helicases displace streptavidin from Biotin-labeled oligonucleotides. Biochemistry *38*, 5164-5171.

Peisley, A., Jo, M., Lin, C., Wu, B., Orme-Johnson, M., Walz, T., Hohng, S., and Hur, S. (2012). Kinetic Mechanism for Viral dsRNA Length Discrimination by MDA5 Filament. Proc Natl Acad Sci U S A *109*, E3340-3349.

Peisley, A., Lin, C., Bin, W., Orme-Johnson, M., Liu, M., Walz, T., and Hur, S. (2011). Cooperative Assembly and Dynamic Disassembly of MDA5 Filaments for Viral dsRNA Recognition. Proc Natl Acad Sci U S A *108*, 21010-21015.

Peisley, A., Wu, B., Yao, H., Walz, T., and Hur, S. (2013). RIG-I Forms Signaling-Competent Filaments in an ATP-Dependent, Ubiquitin-Independent Manner. Mol Cell *51*, 573-583.

Schmid-Burgk, J.L., Schmidt, T., Gaidt, M.M., Pelka, K., Latz, E., Ebert, T.S., and Hornung, V. (2014). OutKnocker: a web tool for rapid and simple genotyping of designer nuclease edited cell lines. Genomes Res *24*, 1719-1723.

Schmid-Burgk, J.L., Schmidt, T., Kaiser, V., Honing, K., and Hornung, V. (2013). A ligation-independent cloning technique for high-throughput assembly of transcription activator–like effector genes. Nat Biotech *31*, 76-81.

Wu, B., Peisley, A., Richards, C., Yao, H., Zeng, X., Lin, C., Chu, F., Walz, T., and Hur, S. (2013). Structural Basis for dsRNA Recognition, Filament Formation, and Antiviral Signal Activation by MDA5. Cell *152*, 276-289.

Wu, B., Peisley, A., Tetrault, D., Li, Z., Egelman, E.H., Magor, K.E., Walz, T., Penczek, P.A., and Hur, S. (2014). Molecular imprinting as a signal activation mechanism of the viral RNA sensor RIG-I. Mol Cell *55*, 511-523.